PCCP

PAPER

View Article Online
View Journal | View Issue

Check for updates

Cite this: *Phys. Chem. Chem. Phys.*, 2024, **26**, 11491

Received 27th January 2024,
Accepted 27th March 2024

DOI: 10.1039/d4cp00391h

rsc.li/pccp

Quantum simulation of conical intersections

Yuchen Wang and David A. Mazziotti *

We explore the simulation of conical intersections (CIs) on quantum devices, setting the groundwork for potential applications in nonadiabatic quantum dynamics within molecular systems. The intersecting potential energy surfaces of H_3^+ are computed from a variance-based contracted quantum eigensolver. We show how the CIs can be correctly described on quantum devices using wavefunctions generated by the anti-Hermitian contracted Schrödinger equation ansatz, which is a unitary transformation of wavefunctions that preserves the topography of CIs. A hybrid quantum-classical procedure is used to locate the seam of CIs. Additionally, we discuss the quantum implementation of the adiabatic to diabatic transformation and its relation to the geometric phase effect. Results on noisy intermediate-scale quantum devices showcase the potential of quantum computers in dealing with problems in nonadiabatic chemistry.

Open Access Article. Published on 08 Abril 2024. Downloaded on 17.02.26 10:47:54.
This article is licensed under a Creative Commons Attribution 3.0 Unported Licence.

1 Introduction

Nonadiabatic processes involve nuclear motion on multiple potential energy surfaces (PESs). These processes are ubiquitous in nature and have been studied extensively in diverse areas such as spectroscopy, solar energy conversion, chemiluminescence, photosynthesis, and photostability of biomolecules.[1–17] Different potential energy surfaces can intersect at regions that exhibit a conical-shaped topography, known as conical intersections (CIs).[18–21] In the vicinity of CIs, the Born–Oppenheimer approximation which assumes adiabaticity breaks down. Systems with nonadiabaticity can undergo sudden changes in their dominant configurations at CIs, leading to the classical and well-known "hop" picture between different electronic states.[22] CIs act as highly efficient channels for converting external excitation energy, usually carried by a photon, to internal electronic energy. Their characterization is crucial to understand rich photochemistry and photobiology processes involving energy conversion.

CIs are in general difficult to treat with quantum mechanical methods for several reasons. First, from the perspective of electronic structure theory, the excited states are harder to compute than the ground state as they correspond to first-order critical points rather than the global minimum. Moreover, the nonunitary ansatz for the wavefunction employed in some methods, such as standard coupled cluster (CC) methods, gives an incorrect topography of CIs.[23–26] Second, since most electronic structure programs work under the Born–Oppenheimer approximation, results obtained from these programs are not readily applicable for subsequent chemical dynamics studies, especially near CIs. The process of converting the original adiabatic electronic structure data to a diabatic representation, referred as diabatization, is an active yet non-unified field due to the non-uniqueness of quasi-diabatic representations.[27–41] Third, the dynamics of nonadiabatic systems typically require a more complex treatment than the dynamics on a single potential energy surface. For example, we need to expand wavefunctions in the basis of every diabatic state to account for effective state transition in quantum dynamics.[1]

Quantum computers could be a natural solution for nonadiabatic chemistry.[42–50] To address some of the concerns in the last paragraph, we observe first that the gate operations are unitary, which makes it convenient to implement a unitary ansatz of wavefunctions (*e.g.*, the unitary coupled cluster (UCC) ansatz[51,52] or the anti-Hermitian contracted Schrödinger equation (ACSE) ansatz[53–61]). They offer robust and accurate solutions to the electronic structure data near CIs. In fact, for the ACSE ansatz used in this paper, classical calculations of CIs are well established.[62–65] Second, quantum computers are ideal tools to perform unitary and even nonunitary propagation[66,67] with a possible polynomial scaling advantage over classical computers where the coupling potential term can be expressed as an entanglement of encoded qubits.[42] Third, the transformation from adiabatic wavefunctions to diabatic wavefunctions is unitary and can be easily implemented as parametric gates during state preparation on quantum computers. The geometric phase,[45,46,68,69] a global phase factor dressing the wavefunctions near CIs, can also be encoded with simple rotations in the Pauli basis, which is a natural advantage of quantum computers.

In this paper we evaluate the performance of quantum computers in describing CIs. Some key issues associated with CIs, such as seam curvature, optimization and geometric phase

Department of Chemistry and The James Franck Institute, The University of Chicago, Chicago, Illinois 60637, USA. E-mail: damazz@uchicago.edu

Open Access Article. Published on 08 Abrèll 2024. Downloaded on 17.02.26 10:47:54.
This article is licensed under a Creative Commons Attribution 3.0 Unported Licence.

are discussed. We implement the electronic structure simulation of H_3^+ with and without noise using the excited-state contracted quantum eigensolver (CQE) proposed in ref. 70 in which the wavefunctions are generated by the ACSE ansatz. The theory and methodology of CI including an overview of CQE are presented in Section 2. Results and outlooks are further discussed in Sections 3 and 4, respectively.

2 Theory

2.1 Diabatic Hamiltonian matrix and CIs

We start from the adiabatic electronic Schrödinger equation,

$$(\hat{H}^a(\mathbf{r};\mathbf{R}) - E_J)|\Psi_J^a(\mathbf{r};\mathbf{R})\rangle = 0 \quad (1)$$

Here, $\mathbf{r}$ and $\mathbf{R}$ denote the electronic and nuclear coordinates and J is a state index. The semicolon indicates that the Hamiltonian is parametrically dependent upon nuclear coordinates arising from the separation of electronic and nuclear degrees of freedom. This approximation, however, fails to describe nonadiabatic dynamics because in the vicinity of conical intersection, different adiabatic wavefunctions produce almost degenerate energies and result in singular derivative coupling vectors, defined below

$$f_{IJ}^a = \langle \Psi_I^a(\mathbf{r};\mathbf{R}')|\hat{\nabla}_{\mathbf{R}}|\Psi_J^a(\mathbf{r};\mathbf{R})\rangle. \quad (2)$$

Under such circumstances it is often necessary to invoke the diabatic representation that produces well-described and smooth state couplings and wavefunctions.[36] The diabatic representation is related to adiabatic representation through a unitary transformation of wavefunction,

$$|\mathbf{\Psi}^d(\mathbf{r};\mathbf{R})\rangle = \mathbf{U}(\mathbf{r};\mathbf{R})|\mathbf{\Psi}^a(\mathbf{r};\mathbf{R})\rangle. \quad (3)$$

If $\mathbf{U}$ is chosen such that $f_{IJ}^d = 0$ everywhere, then we consider the representation strictly diabatic. However, it has been proven that a strict diabatic representation does not exist for polyatomic molecules; hence, we refer to these states as "quasi-diabatic," and the condition for vanishing derivative couplings in the diabatic representation becomes a condition for minimizing $||f_{IJ}^d||$.[27]

The electronic Schrödinger equation can then be rewritten in the diabatic form as

$$[\mathbf{H}^d(\mathbf{R}) - \mathbf{I}E_J(\mathbf{R})]\mathbf{d}_J(\mathbf{R}) = 0 \quad (4)$$

in which $\mathbf{H}^d$ is the quasi-diabatic Hamiltonian matrix, and we omit the dependency of electronic coordinates $\mathbf{r}$ here and below as $\mathbf{H}^d$ is only constructed at each molecular geometry $\mathbf{R}$. The off-diagonal terms of $\mathbf{H}^d$ describes the coupling between different diabatic states, and will be nonzero at most low-symmetry molecular geometries. E_J and $\mathbf{d}_J$ are the eigenvalues and eigenvectors of the Jth state respectively. We consider a two-state example in which $\mathbf{H}^d$ is a two by two matrix throughout this work, where most conclusions can be readily extended to additional electronic states. To obtain degenerate eigenvalues, we require

$$(H_{11} - H_{22})^2 + 4H_{12}H_{21} = 0 \quad (5)$$

where H_{IJ} are matrix elements of $\mathbf{H}^d$.

When wavefunctions are generated from non-Hermitian techniques such as standard coupled cluster methods, the above equation is the only constraint to form CIs. However, this creates a nonphysical $(N-1)$ artifact that accompanies complex eigenvalues in the vicinity of true CIs, where N is the molecular degree of freedom.[23–26] The true CI is a submanifold of the potential energy surfaces where the following two constraint equations, one for diagonal and one for off-diagonal term,

$$H_{11} = H_{22},\ H_{12} = H_{21} = 0 \quad (6)$$

are simultaneously satisfied in the diabatic representation.

It is then easily recognized that the dimension of CIs is $(N-2)$. While the diagonal condition is easy to constrain, the off-diagonal condition is subtle because it is not directly available in electronic structure programs. For some molecules, as we will show in this paper, it is possible to find two states with high symmetry such that the couplings between them are strictly zero by symmetry, a situation known as symmetry-required CIs. The symmetry, however, does not serve as a necessary condition for the existence of CIs as some CIs occur in the more general category of "accidental" CIs.[19]

2.2 Geometric phase effect

Most modern quantum chemistry programs assume the Born–Oppenheimer approximation and thus, produce electronic structure data in the adiabatic representation. Given the limitations of the adiabatic representation in nonadiabatic chemistry, there has been significant research effort directed towards determining the transformation from the adiabatic representation to the diabatic representation. The reason for the abundance of such diabatization techniques is that quasi-diabatic states are not unique.[27] For two-state diabatization, some literature expresses the unitary in eqn (3) as a rotation matrix parameterized by the angle θ,

$$\mathbf{U}(\mathbf{R}) = \begin{pmatrix} \cos\theta(\mathbf{R}) & -\sin\theta(\mathbf{R}) \\ \sin\theta(\mathbf{R}) & \cos\theta(\mathbf{R}) \end{pmatrix}. \quad (7)$$

We remind the reader that the expression might naturally lead to the assumption that θ is a continuous function of $\mathbf{R}$, but this is not necessarily true in the presence of CIs due to the geometric phase effect. The geometric phase effect requires that wavefunctions that are transported around a path enclosing a CI acquire an additional phase factor.[68,71,72] A geometry-dependent and state-dependent factor $e^{iA_K(\mathbf{R})}(K = I,J)$ must be included in the adiabatic wavefunction. The natural advantage of using qubits to represent this two-state diabatization is that both are isomorphic to the special unitary group of degree 2. Indeed on quantum computers, the phase factor can be implemented as a simple rotation gate parametrized by $A_K(\mathbf{R})$. One of

 This journal is © the Owner Societies 2024

Open Access Article. Published on 08 Abrèll 2024. Downloaded on 17.02.26 10:47:54.
This article is licensed under a Creative Commons Attribution 3.0 Unported Licence.

the authors has shown in previous work[73] that $A_J(\mathbf{R})$ can be evaluated from the integral below,

$$A_J(\mathbf{R}) = \oint_{\mathbf{R}_0}^{\mathbf{R}} \left\langle \Psi_I^a(\mathbf{R}') \middle| \hat{\nabla}_{\mathbf{R}'} \middle| \Psi_J^a(\mathbf{R}') \right\rangle \mathrm{d}\mathbf{R}' \tag{8}$$

where the integrand is the derivative coupling vector in eqn (2).[19] As this paper focuses on the topography of CIs, namely a more "static" description, a detailed analysis of the nonadiabatic quantum dynamics, the geometric phase factor and its implementation on quantum platforms is reserved for future work.

2.3 Variance-based contracted quantum eigensolver

The electronic structure calculation in this work is performed with a variance-based contracted quantum eigensolver (CQE) that has been proposed in a previous paper.[70] The algorithm is briefly reviewed here.

The variance (denoted as Var) of the system is defined as:

$$\mathrm{Var}[\Psi_m[{}^2F_m]] = \langle \Psi_m | (\hat{H} - E_m)^2 | \Psi_m \rangle \tag{9}$$

We minimize the variance with respect to the parametric two-body anti-Hermitian operator $\hat{F}_m$, where the wavefunction from ACSE theory at the mth iteration is given by the unitary ansatz as

$$|\Psi_m\rangle = \mathrm{e}^{\hat{F}_m} |\Psi_{m-1}\rangle \tag{10}$$

where

$$\hat{F}_m = \sum_{pqst} {}^2F_m^{pq;st} \hat{a}_p^\dagger \hat{a}_q^\dagger \hat{a}_t \hat{a}_s \tag{11}$$

in which $\hat{a}_p^\dagger$ and $\hat{a}_p$ are the creation and annihilation operators, respectively. The key equation guiding the optimization is derived by taking the gradient of the variance with respect to $\hat{F}_m$:

$$\frac{\partial Var}{\partial \left({}^2F_m^{st;pq}\right)} = 2\langle \Psi_m | \left(\hat{\Gamma}_{st}^{pq} - {}^2D_{st}^{pq} \right) \left(\hat{H} - E_m \right)^2 | \Psi_m \rangle, \tag{12}$$

in which $\hat{\Gamma}_{st}^{pq} = \hat{a}_p^\dagger \hat{a}_q^\dagger \hat{a}_t \hat{a}_s$ and the equation

$${}^2D_{st}^{pq} = \langle \Psi_m | \hat{\Gamma}_{st}^{pq} | \Psi_m \rangle. \tag{13}$$

defines the elements of the two-electron reduced density matrix (2-RDM). Through a self-consistent update of energy and ${}^2F_m$, we can converge the variance to a minima which corresponds to an excited or ground state. More details including an ancillary-assisted measurement of the variance has been reported in previous work.[70]

We provide additional comments regarding why variance-based CQE is suitable to describe the CIs. The convergence depends on the choice of the initial guess, which can be generated from single Slater determinant or a linear combination of them. It will converge to the nearest minimum of the variance without knowledge of the lower states. Here by nearest, we mean the most similar in configuration composition. This state-specific feature can be beneficial in studying the CIs. It allows us to tackle a specific state during the slow variation of molecular geometry without concern that the adiabatic states will cross. Note this also coincides with the idea of configurational-uniformity-based diabatization as first proposed by Nakamura and Truhlar.[29]

3 Results

We demonstrate the approach to computing the CI with the molecule H_3^+. The relative positions of the three co-planar hydrogen atoms are described in polar coordinates as $(R,0)$, (R,π) and (ρ,θ) where $R \geq 0$, $\rho \geq 0$, $0 \leq \theta < 2\pi$, allowing us to represent the molecular geometry by the set of coordinates (R,ρ,θ). Distances are given in the atomic unit bohr unless specified otherwise. Calculations are performed with the IBM Quantum statevector simulator and FakeLagosV2 backend. The statevector simulation is performed without noise, while the fake backend mimics the noise behavior of the real IBM quantum computer Lagos. The quantum simulation result is benchmarked with full configuration interaction calculations. All computations are performed in the minimal Slater-type orbital (STO-3G) basis set. The one- and two-electron integrals are obtained with Maple Quantum Chemistry Package.[74,75] Here and below we denote full configuration interaction as FCI to distinguish it from the abbreviation for the conical intersection (CI).

3.1 Electronic structure of H_3^+

The H_3^+ molecule exhibits arguably the simplest CI. Nonetheless, despite its simplicity, the molecule is an important species in astrochemistry, providing a useful benchmark for the study of CIs.[76–83] We compute the first three states of H_3^+ with $S_z = 0$. A compact mapping is used to reduce the number of required qubits to three for the first and second excited states (denoted as E_1 and E_2) of H_3^+. The mapping is described here. We denote the configuration state function as $|ij\rangle$, $(1 \leq i, j \leq 3)$ with the $S_z = +1/2$ electron occupying the ith molecular orbital and the $S_z = -1/2$ electron occupying the jth molecular orbital. The dimension of FCI matrix is 9. A further reduction is performed by eliminating $|11\rangle$ by observing that it has almost no coupling to the E_1 and E_2 states. Although $|11\rangle$ can couple to other higher states and in principle affect the diagonalization result, the truncation has negligible effect on the energy of E_1 and E_2 ($<10^{-8}$ Hartree), resulting in a total qubit number of $\log_2 8 = 3$.

We analyze the electronic structure property of H_3^+ using the highly-symmetric D_{3h} point group. The first and second excited states correspond to the two components of an E′ irreducible representation and thus form the symmetry-required CIs. We plot the potential energy curve in Fig. 1 obtained from the statevector simulator and a fake-backend simulator. A zoomed region of the degeneracy is given in the figure as well. The two excited states always overlap in the FCI scheme, which is consistent with our electronic structure knowledge of the system. On a noiseless statevector simulator we achieve an energy accuracy of 10^{-6} Hartree, where the only error comes from the trotterization, proving the exactness of the ACSE

Open Access Article. Published on 08 Abril 2024. Downloaded on 17.02.26 10:47:54.
This article is licensed under a Creative Commons Attribution 3.0 Unported Licence.

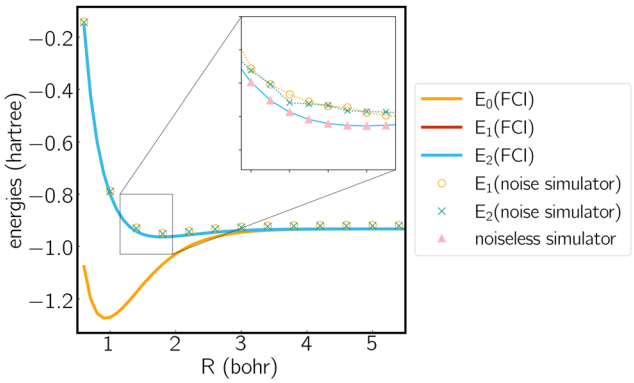

Fig. 1 Potential energy curve calculated by FCI as well as noiseless and noise simulators. Molecule is treated in the D_{3h} symmetry, where the polar coordinates of the three hydrogen atoms are $(R,0)$, (R,π) and $(\sqrt{3}R,\pi/2)$. Note that E_1 and E_2 are degenerate in FCI result due to symmetry.

ansatz. After introducing device noise, the error for each individual state is around 12 mhartree. It is worth noting that since the error is quite uniform for both states, the error of their energy gap is significantly smaller, which is quite promising for predicting the energetic degeneracy.

We next plot the dissociation curve at a lower symmetry, namely C_{2v} in Fig. 2. The discontinuity of the E_2 curve is due to crossings with intruder states. We are particularly interested in the CIs between E_1 and E_2, where the two states coincide at a D_{3h} geometry. Despite the relatively large error of individual states, the prediction of the location of the CIs is surprisingly accurate (<0.01 bohr). As mentioned before, if the error induced by noise is nearly uniform for both states and for all geometries, then the effect of noise is only to shift both potential energy surfaces by a similar amount, which should not significantly affect the topography of the CIs. To verify this, in Fig. 3 we plot the coupled potential energy surfaces as a function of the coordinates of the third hydrogen atom. It can be seen that the topography of the CIs is well reproduced. The expected cusps induced by random noise are barely discernible due to the uniformity of noise. We note, however, that although the potential energy surfaces and relative energy gap are well

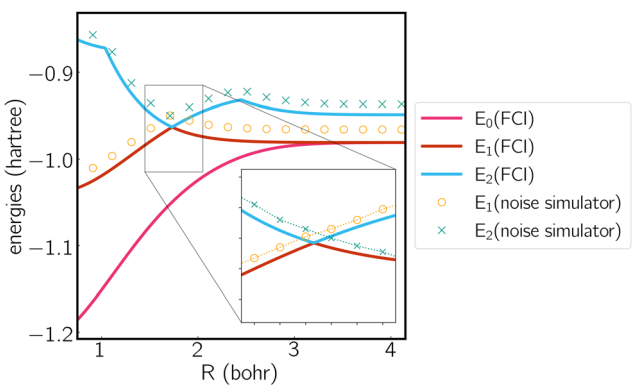

Fig. 2 Potential energy curve calculated by FCI and the noise simulator. Molecule is treated in the C_{2v} symmetry, where the polar coordinates of the three hydrogen atoms are $(1,0)$, $(1,\pi)$ and $(R,\pi/2)$.

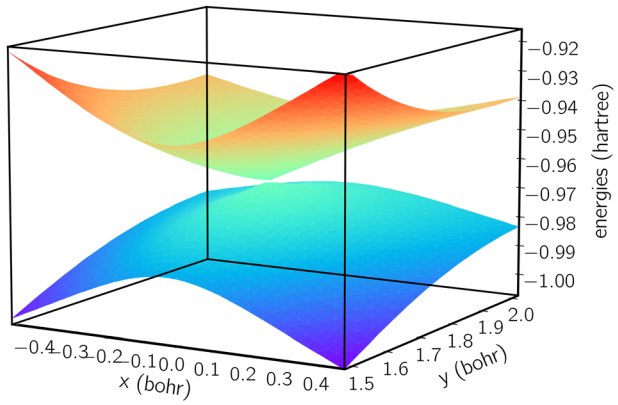

Fig. 3 Intersecting adiabatic potential energy surfaces calculated from variance CQE. The grid size is 20 × 12. Additional points are placed in the vicinity of the CI. For better illustration, we use Cartesian coordinate with the coordinates of the three atoms being $(-1,0,0)$, $(1,0,0)$ and $(x,y,0)$. Unit is bohr.

reproduced, the absolute error still remains challenging on noise intermediate-scale quantum (NISQ) devices and further error mitigation techniques are needed.

3.2 Locating the seam of CI

The search of the minimum energy CI (MEX) is done by minimizing the constrained Lagrangian proposed in previous works,[84,85]

$$L_{IJ}(\mathbf{R}) = E_I(\mathbf{R}) + \lambda_0 \Delta E_{IJ}(\mathbf{R}) + \sum_{k=1}^{M} \lambda_k C_k(\mathbf{R}) \qquad (14)$$

where $\lambda_{0,\ldots,k}$ are Lagrangian multipliers and I, J are state indexes. $\Delta E_{IJ} = E_I - E_J = 0$ is the energy constraint equation for CIs. The significance of the energy constraint is to ensure that we are minimizing the energies while staying within the degenerate subspace. C_k are additional geometry constraint equations; for example, bond length constraints used in this work can be written as $C_k = \mathbf{R}_{pq}{}^2 - c^2$, where $\mathbf{R}_{pq} = \mathbf{R}_p - \mathbf{R}_q$ is the distance between atom p and q.

In a previous paper, we showed that the gradient of Lagrangian corresponding to the geometry parameter set $\mathbf{R}$ can be obtained with classical calculations.[85] Here we use a hybrid method, where single-point energy calculations are performed with the variance-based CQE and the energy gradient is obtained by performing calculations at different geometries and then taking finite differences with a stepsize of 0.1.

The dimension of CI for the triatomic molecule is only one. By varying one molecular coordinate and fixing the rest, we should obtain a one-dimensional curve that corresponds to the seam of the CI. For the special case between the E_1 and E_2 of H_3^+, we know that this curve is unique and corresponds to the D_{3h} geometries in Fig. 1. We report the optimization results by setting R to 2.0 bohr and optimizing over the position of the third hydrogen (r,θ). We use a gradient-like Newton–Raphson method with fixed step size of 0.1 where the Hessian of the Lagrangian is approximated by the identity matrix.

This journal is © the Owner Societies 2024

Open Access Article. Published on 08 Abril 2024. Downloaded on 17.02.26 10:47:54.
This article is licensed under a Creative Commons Attribution 3.0 Unported Licence.

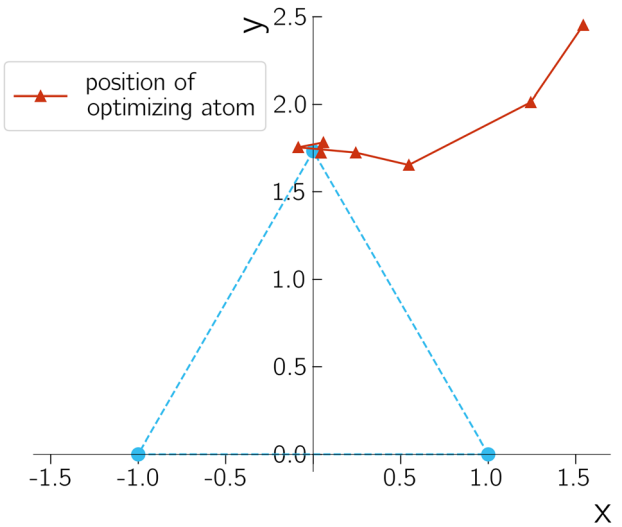

Fig. 4 Trajectory of the unfixed hydrogen atom during optimization. The desired D_{3h} geometry is indicated with blue dots. Cartesian coordinate is used for plotting with the coordinates of the two fixed hydrogen atoms being (−1,0,0), (1,0,0) and the optimizing one being (*x*,*y*,0). Unit is bohr.

Table 1 Energy gap during a geometry optimization with respect to θ and ρ starting from random guesses for these variables. The remaining parameter R is fixed at 1.0 bohr

Iteration number	θ (°)	ρ (bohr)	ΔE (Hartree)
0	57.819	2.897	0.044
1	58.293	2.364	0.066
2	71.721	1.741	0.063
3	81.977	1.741	0.032
4	92.807	1.756	0.014
5	88.136	1.783	0.009
6	88.537	1.724	0.005
Exact	90	1.732	0

A typical optimization process is shown in Fig. 4 by plotting the trajectory of the third unfixed hydrogen atom along the iterations. The geometry parameter and energy difference are reported in Table 1. The performance is quite robust despite the simple setup, suggesting the gradient from quantum devices is resilient enough for geometry optimization purposes. The energy difference decreases during the optimization, except in the first iteration. This exception can occur because the Lagrangian includes contributions beyond the energy difference. An important observation is that, the noise on NISQ simulators introduces a small oscillation around our targeted D_{3h} CI. The errors in the bond distance and bond angle, however, are quite small, which helps to demonstrate the accuracy of our description of the CIs.

4 Conclusions and outlook

Current state-of-art nonadiabatic quantum dynamics are limited to small molecules due to their exponential scaling with respect to the active vibrational modes. Quantum computers may potentially provide a solution. In the future quantum devices with hundreds of qubits may be able to perform nonadiabatic quantum dynamics simulations that are either too expensive or intractable on high-performance classical computers. This paper provides a foundation for simulating the CIs on quantum computers, paving the way for advancements in quantum-based simulations for nonadiabatic molecular systems. Using a variance-based CQE, the energies of intersecting potential energy surfaces of molecular H_3^+ are accurately computed. The study achieves a correct representation of CI topography through a wavefunction generated by a unitary ansatz from ACSE theory. Future work includes realizing diabatization and quantum dynamics of complex nonadiabatic molecular system on quantum devices.

Conflicts of interest

The authors declare no competing financial interest.

Acknowledgements

Y. W. acknowledges helpful discussion with Dr Yafu Guan and Prof. David R. Yarkony. D. A. M. gratefully acknowledges the Department of Energy, Office of Basic Energy Sciences Grant DE-SC0019215, the U.S. National Science Foundation Grant CHE-2155082, and the U.S. National Science Foundation Grant RAISE-QAC-QSA, Grant DMR-2037783. We acknowledge the use of IBM Quantum services for this work. The views expressed are those of the authors and do not reflect the official policy or position of IBM or the IBM Quantum team.

Notes and references

1 H. Guo and D. R. Yarkony, *Phys. Chem. Chem. Phys.*, 2016, **18**, 26335–26352.
2 B. J. Schwartz, E. R. Bittner, O. V. Prezhdo and P. J. Rossky, *J. Chem. Phys.*, 1996, **104**, 5942–5955.
3 B. G. Levine and T. J. Martnez, *Annu. Rev. Phys. Chem.*, 2007, **58**, 613–634.
4 P. V. Demekhin and L. S. Cederbaum, *J. Chem. Phys.*, 2013, **139**, 154314.
5 J. E. Subotnik, A. Jain, B. Landry, A. Petit, W. Ouyang and N. Bellonzi, *Annu. Rev. Phys. Chem.*, 2016, **67**, 387–417.
6 T. E. Li, B. Cui, J. E. Subotnik and A. Nitzan, *Annu. Rev. Phys. Chem.*, 2022, **73**, 43–71.
7 B. F. Curchod and T. J. Martnez, *Chem. Rev.*, 2018, **118**, 3305.
8 S. Matsika, *J. Phys. Chem. A*, 2004, **108**, 7584–7590.
9 S. Matsika and P. Krause, *Annu. Rev. Phys. Chem.*, 2011, **62**, 621.
10 Q. L. Nguyen, V. A. Spata and S. Matsika, *Phys. Chem. Chem. Phys.*, 2016, **18**, 20189–20198.
11 M. S. Schuurman and A. Stolow, *Annu. Rev. Phys. Chem.*, 2018, **69**, 427.
12 Y. Guan, C. Xie, D. R. Yarkony and H. Guo, *Phys. Chem. Chem. Phys.*, 2021, **23**, 24962–24983.
13 Y. Wang, H. Guo and D. R. Yarkony, *Phys. Chem. Chem. Phys.*, 2022, **24**, 15060–15067.

Open Access Article. Published on 08 Abrèll 2024. Downloaded on 17.02.26 10:47:54.
This article is licensed under a Creative Commons Attribution 3.0 Unported Licence.

14 J.-G. Zhou, Y. Shu, Y. Wang, J. Leszczynski and O. Prezhdo, *J. Phys. Chem. Lett.*, 2024, **15**, 1846–1855.
15 M. Baer, *Phys. Rep.*, 2002, **358**, 75–142.
16 B. Mukherjee, K. Naskar, S. Mukherjee, S. Ghosh, T. Sahoo and S. Adhikari, *Int. Rev. Phys. Chem.*, 2019, **38**, 287–341.
17 K. Naskar, S. Mukherjee, B. Mukherjee, S. Ravi, S. Mukherjee, S. Sardar and S. Adhikari, *J. Chem. Theory Comput.*, 2020, **16**, 1666–1680.
18 H. Köuppel, W. Domcke and L. Cederbaum, *Adv. Chem. Phys.*, 1984, 59–246.
19 D. R. Yarkony, *Rev. Mod. Phys.*, 1996, **68**, 985.
20 W. Domcke, D. Yarkony and H. Köppel, *Conical intersections: Electronic structure, dynamics & spectroscopy*, World Scientific, 2004, vol. 15.
21 W. Domcke and D. R. Yarkony, *Annu. Rev. Phys. Chem.*, 2012, **63**, 325.
22 J. C. Tully, *J. Chem. Phys.*, 1990, **93**, 1061.
23 A. Köhn and A. Tajti, *J. Chem. Phys.*, 2007, **127**, 044105.
24 S. Gozem, F. Melaccio, A. Valentini, M. Filatov, M. Huix-Rotllant, N. Ferre, L. M. Frutos, C. Angeli, A. I. Krylov and A. A. Granovsky, *et al.*, *J. Chem. Theory Comput.*, 2014, **10**, 3074.
25 S. Faraji, S. Matsika and A. I. Krylov, *J. Chem. Phys.*, 2018, **148**, 044103.
26 S. Thomas, F. Hampe, S. Stopkowicz and J. Gauss, *Mol. Phys.*, 2021, **119**, e1968056.
27 C. A. Mead and D. G. Truhlar, *J. Chem. Phys.*, 1982, **77**, 6090.
28 K. Ruedenberg and G. J. Atchity, *J. Chem. Phys.*, 1993, **99**, 3799.
29 H. Nakamura and D. G. Truhlar, *J. Chem. Phys.*, 2001, **115**, 10353.
30 W. Eisfeld and A. Viel, *J. Chem. Phys.*, 2005, **122**, 204317.
31 D. Opalka and W. Domcke, *J. Chem. Phys.*, 2013, **138**, 224103.
32 T. Lenzen and U. Manthe, *J. Chem. Phys.*, 2017, **147**, 084105.
33 R. J. Cave and M. D. Newton, *Chem. Phys. Lett.*, 1996, **249**, 15.
34 A. J. Dobbyn and P. J. Knowles, *Mol. Phys.*, 1997, **91**, 1107.
35 C. R. Evenhuis and M. A. Collins, *J. Chem. Phys.*, 2004, **121**, 2515–2527.
36 D. R. Yarkony, C. Xie, X. Zhu, Y. Wang, C. L. Malbon and H. Guo, *Comput. Theor. Chem.*, 2019, **1152**, 41.
37 Y. Wang, Y. Guan and D. R. Yarkony, *J. Phys. Chem. A*, 2019, **123**, 9874.
38 S. Han, Y. Wang, Y. Guan, D. R. Yarkony and H. Guo, *J. Chem. Theory Comput.*, 2020, **16**, 6776.
39 C. Li, S. Hou and C. Xie, *J. Chem. Theory Comput.*, 2023, **19**, 3063.
40 J. Wang, F. An, J. Chen, X. Hu, H. Guo and D. Xie, *J. Chem. Theory Comput.*, 2023, **19**, 2929.
41 E. Vandaele, M. Mališ and S. Luber, *J. Chem. Theory Comput.*, 2024, **20**, 856–872.
42 P. J. Ollitrault, G. Mazzola and I. Tavernelli, *Phys. Rev. Lett.*, 2020, **125**, 260511.
43 P. J. Ollitrault, A. Miessen and I. Tavernelli, *Acc. Chem. Res.*, 2021, **54**, 4229–4238.
44 J. Whitlow, Z. Jia, Y. Wang, C. Fang, J. Kim and K. R. Brown, *Nat. Chem.*, 2023, 1–6.
45 C. H. Valahu, V. C. Olaya-Agudelo, R. J. MacDonell, T. Navickas, A. D. Rao, M. J. Millican, J. B. Pérez-Sánchez, J. Yuen-Zhou, M. J. Biercuk, C. Hempel, T. R. Tan and I. Kassal, *Nat. Chem.*, 2023, **15**, 1503–1508.
46 C. S. Wang, N. E. Frattini, B. J. Chapman, S. Puri, S. M. Girvin, M. H. Devoret and R. J. Schoelkopf, *Phys. Rev. X*, 2023, **13**, 011008.
47 S. Yalouz, B. Senjean, J. Günther, F. Buda, T. E. OBrien and L. Visscher, *Quantum Sci. Technol.*, 2021, **6**, 024004.
48 S. Yalouz, E. Koridon, B. Senjean, B. Lasorne, F. Buda and L. Visscher, *J. Chem. Theory Comput.*, 2022, **18**, 776–794.
49 K. Omiya, Y. O. Nakagawa, S. Koh, W. Mizukami, Q. Gao and T. Kobayashi, *J. Chem. Theory Comput.*, 2022, **18**, 741–748.
50 S. Zhao, D. Tang, X. Xiao, R. Wang, Q. Sun, Z. Chen, X. Cai, Z. Li, H. Yu and W.-H. Fang, 2024, arXiv:*2402.12708*.
51 A. Anand, P. Schleich, S. Alperin-Lea, P. W. Jensen, S. Sim, M. Daz-Tinoco, J. S. Kottmann, M. Degroote, A. F. Izmaylov and A. Aspuru-Guzik, *Chem. Soc. Rev.*, 2022, **51**, 1659.
52 J. Lee, W. J. Huggins, M. Head-Gordon and K. B. Whaley, *J. Chem. Theory Comput.*, 2018, **15**, 311.
53 D. A. Mazziotti, *Phys. Rev. Lett.*, 2006, **97**, 143002.
54 D. A. Mazziotti, *Phys. Rev. A*, 2007, **75**, 022505.
55 D. A. Mazziotti, *Phys. Rev. A: At., Mol., Opt. Phys.*, 2007, **76**, 052502.
56 S. E. Smart and D. A. Mazziotti, *Phys. Rev. Lett.*, 2021, **126**, 070504.
57 S. E. Smart and D. A. Mazziotti, *J. Chem. Theory Comput.*, 2022, **18**, 5286–5296.
58 J.-N. Boyn and D. A. Mazziotti, *J. Chem. Phys.*, 2021, **154**, 134103.
59 J.-N. Boyn, A. O. Lykhin, S. E. Smart, L. Gagliardi and D. A. Mazziotti, *J. Chem. Phys.*, 2021, **155**, 244106.
60 S. E. Smart, J.-N. Boyn and D. A. Mazziotti, *Phys. Rev. A*, 2022, **105**, 022405.
61 Y. Wang, L. M. Sager-Smith and D. A. Mazziotti, *New J. Phys.*, 2023, **25**, 103005.
62 J. W. Snyder, A. E. Rothman, J. J. Foley and D. A. Mazziotti, *J. Chem. Phys.*, 2010, **132**, 154109.
63 J. W. Snyder and D. A. Mazziotti, *J. Chem. Phys.*, 2011, **135**, 024107.
64 J. W. Snyder and D. A. Mazziotti, *J. Phys. Chem. A*, 2011, **115**, 14120–14126.
65 J. W. Snyder and D. A. Mazziotti, *Phys. Chem. Chem. Phys.*, 2011, **14**, 1660–1667.
66 A. W. Schlimgen, K. Head-Marsden, L. M. Sager, P. Narang and D. A. Mazziotti, *Phys. Rev. Lett.*, 2021, **127**, 270503.
67 Z. Hu, R. Xia and S. Kais, *Sci. Rep.*, 2020, **10**, 3301.
68 H. C. Longuet-Higgins, U. Öpik, M. H. L. Pryce and R. Sack, *Proc. R. Soc. London, Ser. A*, 1958, **244**, 1–16.
69 E. Koridon, J. Fraxanet, A. Dauphin, L. Visscher, T. E. O'Brien and S. Polla, *Quantum*, 2024, **8**, 1259.
70 Y. Wang and D. A. Mazziotti, *Phys. Rev. A*, 2023, 022814.
71 C. A. Mead, *Rev. Mod. Phys.*, 1992, **64**, 51.

 This journal is © the Owner Societies 2024

Open Access Article. Published on 08 Abril 2024. Downloaded on 17.02.26 10:47:54.
This article is licensed under a Creative Commons Attribution 3.0 Unported Licence.

72 C. Xie, C. L. Malbon, H. Guo and D. R. Yarkony, *Acc. Chem. Res.*, 2019, **52**, 501–509.
73 Y. Wang and D. R. Yarkony, *J. Chem. Phys.*, 2021, **155**, 174115.
74 Maple, (Maplesoft, Waterloo, 2023).
75 RDMChem, Quantum Chemistry Package (Maplesoft, Waterloo, 2023).
76 H. Kamisaka, W. Bian, K. Nobusada and H. Nakamura, *J. Chem. Phys.*, 2002, **116**, 654.
77 L. P. Viegas, A. Alijah and A. J. Varandas, *J. Chem. Phys.*, 2007, **126**, 074309.
78 P. Barragán, L. Errea, A. Macas, L. Méndez, I. Rabadán and A. Riera, *J. Chem. Phys.*, 2006, **124**, 184303.
79 S. Mukherjee, D. Mukhopadhyay and S. Adhikari, *J. Chem. Phys.*, 2014, **141**, 204306.
80 S. Ghosh, S. Mukherjee, B. Mukherjee, S. Mandal, R. Sharma, P. Chaudhury and S. Adhikari, *J. Chem. Phys.*, 2017, **147**, 074105.
81 Z. Yin, B. J. Braams, B. Fu and D. H. Zhang, *J. Chem. Theory Comput.*, 2021, **17**, 1678.
82 Y. Guan, D. R. Yarkony and D. H. Zhang, *J. Chem. Phys.*, 2022, **157**, 014110.
83 S. Kwon, S. Sandhu, M. Shaik, J. Stamm, J. Sandhu, R. Das, C. V. Hetherington, B. G. Levine and M. Dantus, *J. Phys. Chem. A*, 2023, **127**, 8633–8638.
84 M. R. Manaa and D. R. Yarkony, *J. Chem. Phys.*, 1993, **99**, 5251–5256.
85 Y. Wang and D. R. Yarkony, *J. Chem. Phys.*, 2018, **149**, 154108.